# Spectrum of digitized QCD: Glueballs in a $S(1080)$ gauge theory

Andrei Alexandru,[1,2,*] Paulo F. Bedaque,[2,†] Ruairí Brett,[1,‡] and Henry Lamm[3,§]

[1]*Physics Department, The George Washington University, Washington, DC 20052, USA*
[2]*Department of Physics, University of Maryland, College Park, Maryland 20742, USA*
[3]*Fermi National Accelerator Laboratory, Batavia, Illinois 60510, USA*

(Received 11 January 2022; accepted 31 May 2022; published 15 June 2022)

Quantum simulations of QCD require digitization of the infinite-dimensional gluon field. Schemes for doing this with the minimum amount of qubits are desirable. We present a practical digitization for $SU(3)$ gauge theories via its discrete subgroup $S(1080)$. Using a modified action that allows classical simulations down to $a \approx 0.08$ fm, the low-lying glueball spectrum is computed with percent-level precision at multiple lattice spacings and is shown to extrapolate to the continuum limit $SU(3)$ results. This suggests that this digitization scheme is sufficient for precision quantum simulations of QCD.

DOI: 10.1103/PhysRevD.105.114508

## I. INTRODUCTION

Numerous observables remain firmly beyond the reach of numerical nonperturbative field theory [1–3] due to the sign problem. Sign problems arise when the imaginary time (Euclidean) action of the system is complex or when a real time representation is required. Finite density problems (like the calculation of the equation of state of dense QCD matter or the Hubbard model away from half-filling) are famous examples of the first case; thermalization is an example of the second.

Due to the importance of these problems much effort has been spend on solving or bypassing the sign problem. Quantum computers are a promising avenue leading to a solution to these problems. The time development of the quantum system can be directly mapped into the time evolution of the quantum computer obviating the need for imaginary time calculations. The subtle interference patterns appearing on real time evolution are mimicked by the same pattern inside the quantum computer.

Besides the obvious technological difficulty of building quantum computers, conceptual questions must be answered before quantum field theory can be simulated. First, the state of the system needs to be mapped into a finite—and likely small—quantum register. Then the initial state needs to be prepared, the Hamiltonian evolution coded in terms of elementary gates and, finally, observables must be measured. This paper focuses on the first step, the encoding of the states in the quantum register. The difficulty arises mainly in bosonic theories. Indeed, purely fermionic theories have an infinite dimensional Hilbert space but the usual discretization of space into a finite lattice suffices to reduce the dimensionality to a finite number mappable into a quantum register. However, the Hilbert space of a bosonic fields defined in a single lattice point is already infinite dimensional. Thus, further discretization of *field space* is required to map bosons into a digital quantum register. A wide array of solutions exist [4–14]. Different digitizations break different symmetries of the model [5,5,7,15]. With these reductions, the universality class of the lattice model may differ from the original theory [16–23] making the continuum space limit problematic. Recently, studies quantified the truncation errors for quantum simulations of lattice theories from a computational complexity perspective [12,24–26].

Here, we will investigate the discrete subgroup approximation [27–30] using classical lattice simulations in the action formulation. In contrast, a quantum simulation is likely to be performed in the Hamiltonian formulation. The connection between the two formulations can be derived theoretically via the transfer matrix [31–35] or numerically through taking the anisotropic limit of the action [36–41]. Further, while our simulations were performed in imaginary time, this nonperturbative study of truncation errors is known to be related to those in real time [42–44], thus providing us access to much larger systems than with current quantum devices. Discrete subgroups were studied in the early days of lattice field theory when memory limitations restricted the feasible lattice volumes due to the cost of storing $SU(3)$ elements.

*aalexan@gwu.edu
†bedaque@umd.edu
‡rbrett@gwu.edu
§hlamm@fnal.gov

Replacing a continuous symmetry with a discrete (and smaller) may easily destroy the proper (spacetime) continuum limit. In asymptotically free theories like QCD, the continuum limit is obtained as the inverse coupling $\beta$ diverges while the lattice spacing $a$ goes to zero. However, for $a$ smaller than a certain threshold $a_f$ the discrete theory differs drastically from the one with a continuous group (although there are counterexamples [45]). In the language of euclidean path integrals, the field configurations are "frozen" on the configurations with the minimal action, with the other configurations, due to the gap in action, being exponentially suppressed. This freezing is not necessarily fatal provided we reach the scaling regime: realistic lattice calculations are performed on classical computers with a finite $a$ and extrapolated to $a \to 0$. In these calculations, $a$ should be smaller than typical hadronic scales with modern values of $\mathcal{O}(0.1\text{ fm})$.

Subgroups of $U(1)$ [46–48] and $SU(N)$ [49–56] gauge fields—including with fermions [57,58]—were tested with differing degrees of success. In particular, all five crystal-like subgroups of $SU(3)$ freeze before the scaling regime with the Wilson action [28,51,53]. Subsequent work increased the phase transition by including the midpoints between elements of $S(1080)$ [54]. However, this procedure breaks gauge symmetry. An alternative proposal studied for $U(1)$ chooses an optimized subset of group elements [59,60].

Introducing new terms to the discrete action can decrease $a_f$. The new action has formally the same continuum limit, but it is different at finite lattice spacing. The net effect is that the gap $\delta S$ between the lowest action configurations is lowered and the freezing $a_f$ is reduced. Classical Monte Carlo calculations were performed in [28], finding that $a \approx 0.08$ fm is possible with the addition of a single term to the action. We must check empirically that this action generates the same physics as $SU(3)$ by reproducing continuum IR observables. The previous work [28] demonstrated that the deconfining temperature of pure-glue $SU(3)$ was reproduced in the continuum from $S(1080)$ to subpercent accuracy. In order to argue for the usefulness of this approach to quantum simulations we need verify that the $S(1080)$ is capable of reproducing the hadronic spectrum. Here, we show that percent-level accuracy can be achieved for the low-lying glueball states, the massive excitations of pure-glue SU(3).

## II. THEORY

In this work, we use the action proposed in [28]:

$$S[U] = -\sum_p \left( \frac{\beta_0}{3} \mathrm{ReTr}(U_p) + \beta_1 \mathrm{ReTr}(U_p^2) \right), \quad (1)$$

where $U_p$ is a plaquette and $\beta_i$ are coupling constants. Modified actions like Eq. (1) were observed for $U_p \in SU(3)$ to have milder lattice spacing errors [35,61–64] with the same continuum limit as the Wilson action ($S_W = -\frac{\beta_W}{3} \sum_p \mathrm{ReTr} U_p$).

The inability of the discrete field fluctuations to be made arbitrarily small lead to a phase boundary $\{\beta_i\}$ beyond which $S(1080)$ gauge links become frozen to $\mathbb{1}$ while the $SU(3)$ gauge links remain dynamical. In this phase, no clear connection between $S(1080)$ and $SU(3)$ exists. That is what limits the lattice spacing to $a > a_f$. By setting $\beta_1 < 0$ the gap between the values of the frozen and dynamical discrete links is reduced and thus $a_f$ decreased.

In [28] the trajectory $\beta_1 = -0.1267\beta_0 + 0.253$ was found to allow for lattice spacing down to $a \gtrsim 0.08$ fm when computing the Wilson flow parameter $t_0$ [65]. This trajectory was chosen to avoid the freezing transition in a small $2^4$ lattice. This value of $a \gtrsim 0.08$ fm is clearly in the scaling regime where the correlation lengths are much smaller than $a$ and lattice artifacts are small.

## III. METHODOLOGY

To extract glueball masses we need to measure two-point functions of operators with the appropriate quantum numbers. Gluon correlators are noisy and the extraction of gluon masses hinge on a good choice of interpolating fields and a a variational calculation employing a large set of operators. Fortunately, a sophisticated technique has been developed that we can use for glueball spectroscopy [66–71].

While the traditional approach for $SU(3)$ glueball spectroscopy involves anisotropic lattices [68], we used isotropic lattices, to avoid the complication of tuning the anisotropy. These operators need to be gauge invariant and are constructed from traces of *loops*, sets of links that track paths that return to the starting point. The basic seed paths we used for this study are one 4-link long, three 6-link long, and 18 8-links long (Fig. 1). Generically an $n$-link loop operator is given by

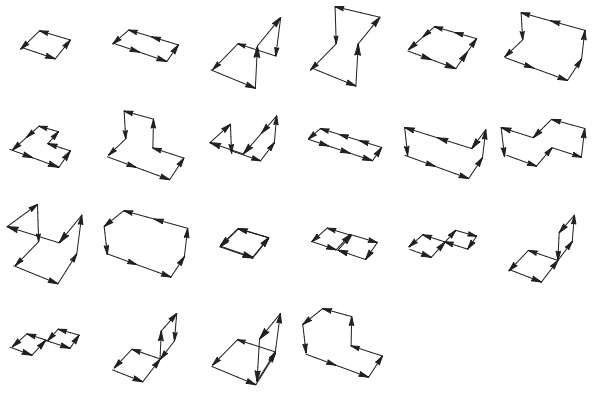

FIG. 1. Seed loops for the operator constructions, using 4, 6, and 8 links.

$$[x;\mu_1,\ldots,\mu_n] \equiv \mathrm{Tr}\prod_{i=1}^{n} U_{\mu_i}\left(x+\sum_{j<i}\mu_j\right). \tag{2}$$

Above, $x$ is the starting point for the loop and $\mu_i$ are *spatial* displacements for the loop. Since this is a loop, the displacements satisfy $\sum_k \mu_k = 0$. The *links* $U_\mu(x)$ represent a Wilson line connecting $x$ and $x+\mu$. As the lattice spacing is reduced the loops are enlarged by *blocking*, that is, repeating the steps in the loop, so that the size of the loops in physical units stays constant. For example $[\mu_1,\mu_2,\ldots,\mu_n]$ can be replaced with $[\mu_1,\mu_1,\mu_2,\mu_2,\ldots,\mu_n,\mu_n]$.

We will consider only zero-momentum operators resulting from summing (2) over $x$. These operators have symmetries that we use to make their calculation more efficient: they are invariant under circular permutations of the steps, and the opposite orientation loop is related to the original one via a complex-conjugation.

The loop operators must be projected onto the appropriate irreducible representations (*irreps*) of the finite-volume symmetry group $O_h$ (we consider only cubic boxes), a subgroup of the infinite-volume symmetry group, $O(3)$. These projectors are given by:

$$P^{\Gamma}_{\lambda\lambda'}\ell \equiv \frac{d_\Gamma}{|G|}\sum_{g\in G}[D^{\Gamma}_{\lambda\lambda'}(g)]^* R(g)\ell, \tag{3}$$

where $\ell = [\mu_1,\ldots,\mu_n]$ and $R\ell = [R\mu_1,\ldots,R\mu_n]$ is the loop transformed by $R$. Above, $d_\Gamma$ is the dimension of the irrep $\Gamma$, $|G|$ is the number of elements in the group, $D^{\Gamma}(g)$ is the matrix associated with element $g$ in irrep $\Gamma$ and $R(g)$ is the three-dimensional representation of $O_h$ (these are the same matrices as $D^{T_1^-}(g)$.) The group $O_h$ has 24 proper rotations, and 24 rotations combined with an inversion. There are 10 irreps: $A_1^{\pm}$, $A_2^{\pm}$, $E^{\pm}$, $T_1^{\pm}$, and $T_2^{\pm}$ with dimensions 1, 1, 2, 3, and 3. The multiplets of $O(3)$ can be decomposed into smaller invariant multiplets of $O_h$. For instance, the scalar ($J=0$) irrep corresponds to the $A_1$ irrep of $O_h$ while the $J=2$ breaks down into $E\oplus T_2$. The parity is the same for both infinite volume and finite volume irreps.

The other quantum number relevant for operator construction is the charge parity. Charge conjugation for the glue fields is given by $U_\mu(x)\to U_\mu(x)^*$, so the loop operators transform similarly $\ell\to\ell^*$. The even-charge operators, which we consider here, correspond to the real part of $\ell$ and the odd ones to the imaginary parts. Finally, in order to increase the overlap of the loop-operators with the glueball states we *stout smear* the links [72].

In our calculation, we used the following operator basis. All loops were computed using smeared operator on blocked links. We used 16 different combinations. For each gauge-configuration we repeatedly smeared the links generating four different smearing levels with $n_{\mathrm{smear}} = 2, 4, 6, 8$. For each smearing set of links we evaluated the loops using blocked links with $n_{\mathrm{block}} = 2, 4, 6, 8$.

Since the gluon correlators becomes noisy at fairly small time separations, a delicate fitting procedure is required to extract the glueball masses. Finite-volume glueball energies are best extracted by computing *matrices* of temporal correlators,

$$C_{ij}(\tau) = \sum_{\tau_0}\langle 0|\mathcal{O}_i(\tau+\tau_0)\mathcal{O}_j(\tau_0)^\dagger|0\rangle, \tag{4}$$

for large sets of glueball operators $\mathcal{O}(\tau) = O(\tau) - \langle 0|O(\tau)|0\rangle$. In practice, the vacuum subtraction only needs to be performed for operators with vacuum quantum numbers, i.e., the $A_1^{++}$ sector. We construct the matrix

$$\tilde{C}(\tau) = U^\dagger C(\tau_0)^{-1/2} C(\tau) C(\tau_0)^{-1/2} U, \tag{5}$$

where the columns of $U$ are the eigenvectors of $G(\tau_d) = C(\tau_0)^{-1/2}C(\tau_d)C(\tau_0)^{-1/2}$. The parameters $\tau_0$ and $\tau_d$, named the pivot and diagonalization times, are chosen such that $\tilde{C}(\tau)$ remains (approximately) diagonal for $\tau > \tau_d$, and the extracted energies are insensitive to parameter variations. The spectrum is then extracted by fitting the diagonal elements $\tilde{C}_{kk}(\tau)$ to the ansatz $A_k[e^{-E_k\tau} + e^{-E_k(T-\tau)}]$, with $T$ the extent of the Euclidean lattice time. The ground state is associated with the largest eigenvalue of $G(\tau_d)$, the first excited state with the second largest eigenvalue, and so on.

From the 22 seed loops in Fig. 1, 626 linearly independent operators are produced across the 20 $\Gamma^C$ symmetry sectors. Performing the smearing and blocking process leads to 10,016 independent operators for the 16 sets of links. While the full set of operators for a given irrep can be used, in practice it is often necessary to carefully prune the operator basis. This is done by removing operators with poor overlap onto the states of interest, and those whose correlators have a low signal-to-noise ratio. Unlike modern QCD calculations [73,74] here we are only interested in the ground state in a given irrep. Therefore, while pruning is helpful in simplifying the analysis to smaller matrices, we find our results insensitive to it.

## IV. RESULTS

Our results are obtained from three $S(1080)$ ensembles using the same couplings as [28]. The parameters were chosen to scan a set $a \in [0.08, 0.16]$ fm. The lattice spacing was determined from $t_0$, the Wilson flow time [65]. A detailed list of parameters is in Table I. These ensembles were generated using a multihit Metropolis update algorithm, which we found to be as efficient as a heat-bath in terms of autocorrelation length but significantly cheaper to implement. For each ensemble we generated around 650,000 independent configurations with sufficient decorrelation steps. Computing time was dominated by measuring the loop-operators, so we used a conservative number of update steps between measurements.

TABLE I. Input parameters. The top three lines are for $S(1080)$ and the forth is the $SU(3)$ calibration run. The parameters are: $\rho$ the stout smearing parameter, $n_{\text{decorr}}$ the number of updates between measurements, $n_\rho$ and $n_b$ the number of smearing and blocking levels respectively. For $S(1080)$, the couplings $\beta_0$ and $\beta_1$ are normalized as in Eq. (1), and follow the trajectory in the text, whereas for $SU(3)$ simulations $\beta_0$ is the Wilson coupling. Observables are quoted in lattice units, with statistical errors only. For $SU(3)$ the value of $\sqrt{t_0}/a$ is from [75].

| $\beta_0$ | $\beta_1$ | $n_x^3 \times n_t$ | $n_{\text{therm}}$ | $n_{\text{decorr}}$ | $\rho$ | $n_{\text{meas}}$ | $n_{\text{bins}}$ | $\sqrt{t_0}/a$ | $am_{A_1^{++}}$ | $am_{A_1^{-+}}$ | $am_{E^{++}}$ |
|---|---|---|---|---|---|---|---|---|---|---|---|
| 9.154 | −0.9065 | $16^3 \times 16$ | 200 | 40 | 0.2 | 652500 | 1305 | 1.016(3) | 1.272(14) | 2.201(35) | 1.986(17) |
| 12.795 | −1.3677 | $16^3 \times 16$ | 200 | 40 | 0.2 | 650000 | 1300 | 1.508(3) | 0.859(13) | 1.386(22) | 1.296(16) |
| 19.61 | −2.2309 | $16^3 \times 16$ | 200 | 40 | 0.2 | 647500 | 1295 | 2.000(4) | 0.6498(84) | 1.071(11) | 0.9644(82) |
| 6.0625 | ⋯ | $16^3 \times 16$ | 200 | 5 | 0.2 | 567500 | 1135 | 1.962(1) | 0.6352(79) | 1.088(12) | 0.9649(84) |

To verify that our operator basis overlaps well with the glueballs and that our fitting method is sound, we carried out a calibration run using an $SU(3)$ ensemble. We generated a set of $SU(3)$ Wilson-gauge configurations for $\beta = 6.0625$ and compare our results with the state-of-the-art calculations of [71] for one value of $\beta$ that is near the lattice spacing on one of our $S(1080)$ ensembles. We generated similar statistics to the $S(1080)$ ensembles and used the same set of operators. The full set of parameters for this run is included in the last row of Table I.

For analysis we binned the measurements in groups of 500, both to remove the possible autocorrelation effects and to make the data analysis more manageable. We fit a single exponential function, $A[e^{-m\tau} + e^{-m(T-\tau)}]$, to the ground state correlator in the time range $\tau \in [\tau_i, \tau_f]$. The relevant parameters for these calculations are in Table II. The masses and their errors were extracted using a correlated fit to take into account the covariance of the correlator at different times. The covariance matrix for the correlator was estimated using the jackknife method. The results are plotted in Fig. 2 and included in Table I.

TABLE II. Analysis parameters for the $S(1080)$ calculation (top rows) and the $SU(3)$ calibration run (bottom). Included are the pivot time $\tau_0$, the diagonalization time $\tau_d$, the fit range $[\tau_i, \tau_f]$, and the $\chi^2$ per degree of freedom.

| $\beta_0$ | Irrep | $\tau_0$ | $\tau_d$ | $\tau_i$ | $\tau_f$ | $\chi^2$/dof |
|---|---|---|---|---|---|---|
| 9.154 | $A_1^{++}$ | 0 | 1 | 2 | 7 | 0.94 |
| | $A_1^{-+}$ | 1 | 2 | 1 | 15 | 0.82 |
| | $E^{++}$ | 0 | 1 | 1 | 15 | 1.37 |
| 12.795 | $A_1^{++}$ | 0 | 1 | 3 | 8 | 1.24 |
| | $A_1^{-+}$ | 0 | 1 | 2 | 7 | 0.96 |
| | $E^{++}$ | 0 | 1 | 2 | 8 | 1.91 |
| 19.61 | $A_1^{++}$ | 0 | 1 | 3 | 8 | 1.47 |
| | $A_1^{-+}$ | 0 | 1 | 2 | 5 | 1.11 |
| | $E^{++}$ | 0 | 1 | 2 | 8 | 0.83 |
| 6.0625 | $A_1^{++}$ | 2 | 3 | 3 | 10 | 1.01 |
| | $A_1^{-+}$ | 0 | 1 | 2 | 7 | 0.90 |
| | $E^{++}$ | 1 | 2 | 2 | 8 | 1.07 |

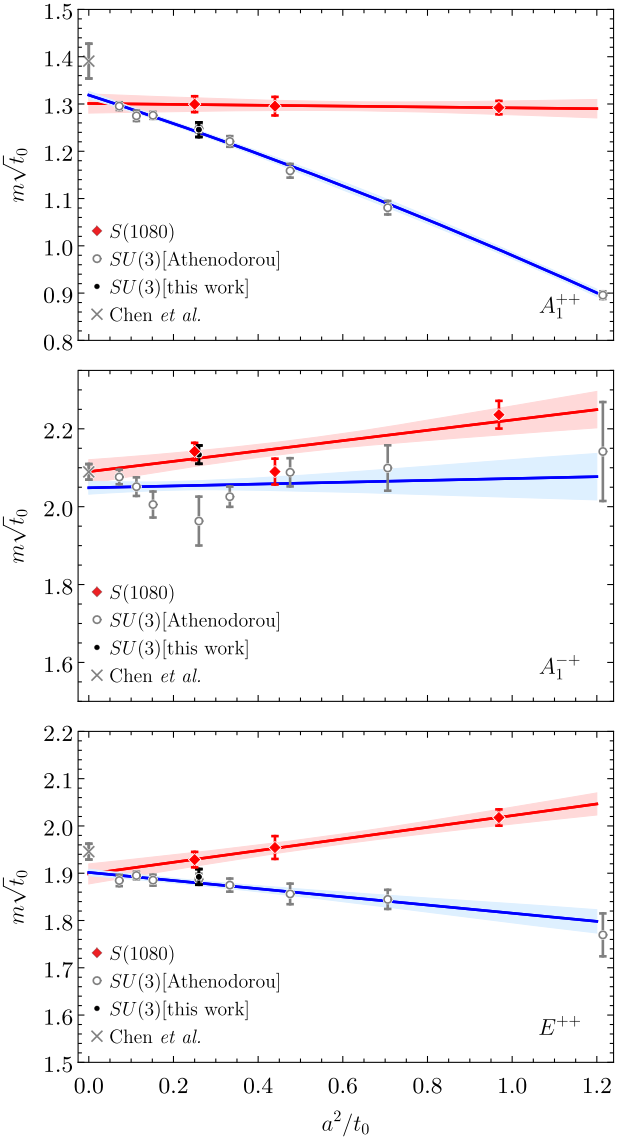


FIG. 2. Masses for $A_1^{++}$ ($J^{PC} = 0^{++}$), $A_1^{-+}$ ($J^{PC} = 0^{-+}$), and $E^{++}$ ($J^{PC}=2^{++}$) glueballs vs $a^2/t_0$. Our $S(1080)$ (filled red diamond) and $SU(3)$ (filled black circle) results compared to $SU(3)$ results from [71] (open gray circle). Another continuum $SU(3)$ result [70] (gray cross) is presented to estimate systematic errors.

TABLE III. $a \to 0$ extrapolations of $m\sqrt{t_0}$, for $S(1080)$ and $SU(3)$ simulations. The results of [71] uses an isotropic lattice whereas [70] use an anisotropic lattice.

| Irrep | $S(1080)$ | $SU(3)$ [71] | $SU(3)$ [70] |
|---|---|---|---|
| $A_1^{++}$ | 1.301(20) | 1.319(8) | 1.391(37) |
| $A_1^{-+}$ | 2.090(31) | 2.049(17) | 2.089(20) |
| $E^{++}$ | 1.899(21) | 1.902(7) | 1.946(17) |

We extracted the glueball masses corresponding to the ground states in the $A_1^{++}$, $E^{++}$, and $A_1^{-+}$ irreps, corresponding to the lowest lying glueballs. The $SU(3)$ calibration run results are included in Fig. 2 and are consistent with those from Ref. [71]. The $A_1^{-+}$ point differs from the corresponding mass from Ref. [71], yet we note that at this point the results from Ref. [71] have large error bars and are at tension with their own continuum extrapolation. Our $S(1080)$ results are extrapolated to $a = 0$ assuming the expected quadratic form $m(a)\sqrt{t_0} = m(0)\sqrt{t_0} + ca^2/t_0$. These extrapolations are indicated in Fig. 2 with a red line and compared with the $SU(3)$ extrapolations from Refs. [70,71]. For our calculations we use $\sqrt{t_0}/a$ values measured directly on these ensembles [28] (see Table I). For the $SU(3)$ results we used the parametrization of $\sqrt{t_0}/a$ as a function of $\beta$ for the pure glue Wilson action included in a recent study [75] and we perform the same continuum extrapolation as in Ref. [71]. To gauge the systematics of the $SU(3)$ calculation, we included the results from an independent calculation [70]. The extrapolation results are included in Table III. As we can see, the results agree within their statistical errors at the percent level. Compared to previous results for the deconfining temperature $T_0\sqrt{t_0} = 0.2489(11)$, our results probe nearly an order of magnitude higher in energy $m\sqrt{t_0} \sim 2$ finding agreement with $SU(3)$ in the continuum. This supports the claim that this modified action reproduces $SU(3)$ physics below 2.5 $\mathrm{GeV}^{-1}$.

## V. CONCLUSIONS

These results provides strong evidence that $S(1080)$ can replace $SU(3)$ in quantum simulations of observables which cannot be computed using classical lattice techniques in imaginary time e.g. [76]. This includes some key QCD phenomena that have remained mysterious up to now like the mechanism of thermalization in heavy ion collisions that is believed to be driven mostly by gluons. The $\mathcal{O}(10^2)$ qubit savings from using an 11-qubit $S(1080)$ register instead of $SU(3)$ compare favorably to other digitizations [14,77–80]. Even with the small lattice sizes dominating the error due to the limited number of qubits, the model studied here represents a sufficient approximation of $SU(3)$ for $a \gtrsim 0.08$ fm in classical simulations. Future work should investigate what effect taking the anisotropic limit has on the minimum lattice spacing, as this has a direct connection to the Hamiltonian. As quantum computers get larger, smaller lattice errors may become desirable. In such case, systematic improvements are possible. Including additional terms in the action proportional to other characters [29,55,56] can allow for smaller $a$, while improved actions, in the spirit of the Symanzik program, can reduce the systemic error for fixed $a$ [81–83]. The relative cost of these two improvements is left for future work. Finally, including dynamical fermions into discrete subgroups simulations should be performed to understand how this full theory compared to QCD. While there is no conceptual issue in including fermions, the numerical value of the minimum lattice size achievable will depend on the number of dynamical quarks.

## ACKNOWLEDGMENTS

A. A. and R. B. are grateful to Andreas Athenodorou for his guidance on constructing a good operator basis for the variational analysis. P. B was supported in part by the US DOE under Contract No. DE-FG02-93ER-40762 and by U.S. DOE Grant No. DE-SC0021143. A. A. is supported in part by the U.S. Department of Energy grant No. DE-FG02-95ER40907. H. L is supported by the Department of Energy through the Fermilab QuantiSED program in the area of "Intersections of QIS and Theoretical Particle Physics". Fermilab is operated by Fermi Research Alliance, LLC under contract No. DE-AC02-07CH11359 with the United States Department of Energy.

[1] R. P. Feynman, Simulating physics with computers, Int. J. Theor. Phys. **21**, 467 (1982).
[2] S. P. Jordan, H. Krovi, K. S. Lee, and J. Preskill, BQP-completeness of scattering in scalar quantum field theory, Quantum **2**, 44 (2018).
[3] M. Carena, H. Lamm, Y.-Y. Li, J. D. Lykken, L.-T. Wang, and Y. Yamauchi, Practical quantum advantages in high energy physics, Snowmass 2021 LOI, TF10-077, 2020.
[4] E. Zohar, J. I. Cirac, and B. Reznik, Cold-Atom Quantum Simulator for SU(2) Yang-Mills Lattice Gauge Theory, Phys. Rev. Lett. **110**, 125304 (2013).
[5] E. Zohar, J. I. Cirac, and B. Reznik, Quantum simulations of gauge theories with ultracold atoms: Local gauge invariance

from angular momentum conservation, Phys. Rev. A **88**, 023617 (2013).
[6] E. Zohar and M. Burrello, Formulation of lattice gauge theories for quantum simulations, Phys. Rev. D **91**, 054506 (2015).
[7] U.-J. Wiese, Towards quantum simulating QCD, Proceedings of the 24th International Conference on Ultra-Relativistic Nucleus-Nucleus Collisions (Quark Matter 2014), Darmstadt, Germany, May 19-24, 2014, Nucl. Phys. **A931**, 246 (2014).
[8] E. Zohar, A. Farace, B. Reznik, and J. I. Cirac, Digital lattice gauge theories, Phys. Rev. A **95**, 023604 (2017).
[9] J. Bender, E. Zohar, A. Farace, and J. I. Cirac, Digital quantum simulation of lattice gauge theories in three spatial dimensions, New J. Phys. **20**, 093001 (2018).
[10] N. Klco, J. R. Stryker, and M. J. Savage, SU(2) non-Abelian gauge field theory in one dimension on digital quantum computers, Phys. Rev. D **101**, 074512 (2020).
[11] I. Raychowdhury and J. R. Stryker, Loop, string, and hadron dynamics in SU(2) Hamiltonian lattice gauge theories, Phys. Rev. D **101**, 114502 (2020).
[12] Z. Davoudi, I. Raychowdhury, and A. Shaw, Search for efficient formulations for Hamiltonian simulation of non-Abelian lattice gauge theories, Phys. Rev. D **104**, 074505 (2021).
[13] M. Kreshchuk, W. M. Kirby, G. Goldstein, H. Beauchemin, and P. J. Love, Quantum simulation of quantum field theory in the light-front formulation, Phys. Rev. A **105**, 032418 (2022).
[14] A. Ciavarella, N. Klco, and M. J. Savage, A trailhead for quantum simulation of SU(3) Yang-Mills lattice gauge theory in the local multiplet basis, Phys. Rev. D **103**, 094501 (2021).
[15] I. Raychowdhury and J. R. Stryker, Solving Gauss's law on digital quantum computers with loop-string-hadron digitization, Phys. Rev. Research **2**, 033039 (2020).
[16] P. Hasenfratz and F. Niedermayer, Asymptotic freedom with discrete spin variables?, in Proceedings of the 2001 Europhysics Conference on High Energy Physics (EPS-HEP 2001), Budapest, Hungary, 2001, Proc. Sci., HEP2001 (**2001**) 229.
[17] S. Caracciolo, A. Montanari, and A. Pelissetto, Asymptotically free models and discrete non-Abelian groups, Phys. Lett. B **513**, 223 (2001).
[18] P. Hasenfratz and F. Niedermayer, Asymptotically free theories based on discrete subgroups, Nucl. Phys. B, Proc. Suppl. **94**, 575 (2001).
[19] A. Patrascioiu and E. Seiler, Continuum limit of two-dimensional spin models with continuous symmetry and conformal quantum field theory, Phys. Rev. E **57**, 111 (1998).
[20] R. Krcmar, A. Gendiar, and T. Nishino, Phase diagram of a truncated tetrahedral model, Phys. Rev. E **94**, 022134 (2016).
[21] A. Alexandru, P. F. Bedaque, H. Lamm, and S. Lawrence (NuQS Collaboration), $\sigma$ Models on Quantum Computers, Phys. Rev. Lett. **123**, 090501 (2019).
[22] S. Caracciolo, A. Montanari, and A. Pelissetto, Asymptotically free models and discrete non-Abelian groups, Phys. Lett. B **513**, 223 (2001).
[23] A. Alexandru, P. F. Bedaque, A. Carosso, and A. Sheng, Universality of a truncated sigma-model, arXiv:2109.07500.
[24] A. F. Shaw, P. Lougovski, J. R. Stryker, and N. Wiebe, Quantum algorithms for simulating the lattice Schwinger model, Quantum **4**, 306 (2020).
[25] A. Kan and Y. Nam, Lattice quantum chromodynamics and electrodynamics on a universal quantum computer, arXiv:2107.12769.
[26] Y. Tong, V. V. Albert, J. R. McClean, J. Preskill, and Y. Su, Provably accurate simulation of gauge theories and bosonic systems, arXiv:2110.06942.
[27] D. C. Hackett, K. Howe, C. Hughes, W. Jay, E. T. Neil, and J. N. Simone, Digitizing gauge fields: Lattice Monte Carlo results for future quantum computers, Phys. Rev. A **99**, 062341 (2019).
[28] A. Alexandru, P. F. Bedaque, S. Harmalkar, H. Lamm, S. Lawrence, and N. C. Warrington (NuQS Collaboration), Gluon field digitization for quantum computers, Phys. Rev. D **100**, 114501 (2019).
[29] Y. Ji, H. Lamm, and S. Zhu (NuQS Collaboration), Gluon field digitization via group space decimation for quantum computers, Phys. Rev. D **102**, 114513 (2020).
[30] M. S. Alam, S. Hadfield, H. Lamm, and A. C. Y. Li, Quantum simulation of dihedral gauge theories, arXiv:2108.13305.
[31] M. Creutz, Gauge fixing, the transfer matrix, and confinement on a lattice, Phys. Rev. D **15**, 1128 (1977).
[32] M. Luscher, Construction of a selfadjoint, strictly positive transfer matrix for Euclidean lattice gauge theories, Commun. Math. Phys. **54**, 283 (1977).
[33] M. Luscher and P. Weisz, Definition and general properties of the transfer matrix in continuum limit improved lattice gauge theories, Nucl. Phys. **B240**, 349 (1984).
[34] X.-Q. Luo, S.-H. Guo, H. Kroger, and D. Schutte, Improved lattice gauge field Hamiltonian, Phys. Rev. D **59**, 034503 (1999).
[35] M. Hasenbusch and S. Necco, SU(3) lattice gauge theory with a mixed fundamental and adjoint plaquette action: Lattice artifacts, J. High Energy Phys. 08 (2004) 005.
[36] C. Hamer, Scales of Euclidean and Hamiltonian lattice gauge theory in three dimensions, Phys. Rev. D **53**, 7316 (1996).
[37] M. Loan, M. Brunner, and C. Hamer, Mass gap in compact $U(1)$ model in $(2+1)$-dimensions, arXiv:hep-lat/0209161.
[38] M. Loan, M. Brunner, C. Sloggett, and C. Hamer, Path integral Monte Carlo approach to the $U(1)$ lattice gauge theory in $(2+1)$-dimensions, Phys. Rev. D **68**, 034504 (2003).
[39] M. Loan, T. Byrnes, and C. Hamer, Hamiltonian study of improved $U(1)$ lattice gauge theory in three dimensions, Phys. Rev. D **70**, 014504 (2004).
[40] T. M. R. Byrnes, M. Loan, C. J. Hamer, F. D. R. Bonnet, D. B. Leinweber, A. G. Williams, and J. M. Zanotti, The Hamiltonian limit of $(3+1)$-D SU(3) lattice gauge theory on anisotropic lattices, Phys. Rev. D **69**, 074509 (2004).
[41] D. Harlow and H. Ooguri, Symmetries in quantum field theory and quantum gravity, Commun. Math. Phys. **383**, 1669 (2021).
[42] K. Osterwalder and R. Schrader, Axioms for Euclidean Green's functions, Commun. Math. Phys. **31**, 83 (1973).

[43] K. Osterwalder and R. Schrader, Axioms for Euclidean Green's functions II, Commun. Math. Phys. **42**, 281 (1975).
[44] M. Carena, H. Lamm, Y.-Y. Li, and W. Liu, Lattice renormalization of quantum simulations, Phys. Rev. D **104**, 094519 (2021).
[45] B. B. Beard, M. Pepe, S. Riederer, and U. J. Wiese, Study of CP($N-1$) $\theta$-Vacua by Cluster-Simulation of SU(N) Quantum Spin Ladders, Phys. Rev. Lett. **94**, 010603 (2005).
[46] M. Creutz, L. Jacobs, and C. Rebbi, Monte Carlo study of Abelian lattice gauge theories, Phys. Rev. D **20**, 1915 (1979).
[47] M. Creutz and M. Okawa, Generalized actions in $Z(p)$ lattice gauge theory, Nucl. Phys. **B220**, 149 (1983).
[48] M. Fukugita, T. Kaneko, and M. Kobayashi, Phase structure and duality of $Z(N)$ lattice gauge theory with generalized actions in four space-time dimensions, Nucl. Phys. **B215**, 289 (1983).
[49] D. Petcher and D. H. Weingarten, Monte Carlo calculations and a model of the phase structure for gauge theories on discrete subgroups of SU(2), Phys. Rev. D **22**, 2465 (1980).
[50] L. Jacobs and C. Rebbi, Multispin coding: A very efficient technique for Monte Carlo simulations of spin systems, J. Comput. Phys. **41**, 203 (1981).
[51] G. Bhanot and C. Rebbi, Monte Carlo simulations of lattice models with finite subgroups of SU(3) as gauge groups, Phys. Rev. D **24**, 3319 (1981).
[52] H. Grosse and H. Kuhnelt, Phase structure of lattice gauge theories for non-Abelian subgroups of SU(3), Phys. Lett. **101B**, 77 (1981).
[53] G. Bhanot, SU(3) lattice gauge theory in four-dimensions with a modified Wilson action, Phys. Lett. **108B**, 337 (1982).
[54] P. Lisboa and C. Michael, Discrete subsets of SU(3) for lattice gauge theory, Phys. Lett. **113B**, 303 (1982).
[55] H. Flyvbjerg, Group space decimation: A way to simulate the 1080 element subgroup of SU(3)?, Nucl. Phys. **B243**, 350 (1984).
[56] H. Flyvbjerg, Internal space decimation for lattice gauge theories, Nucl. Phys. **B240**, 481 (1984).
[57] D. H. Weingarten and D. N. Petcher, Monte Carlo integration for lattice gauge theories with fermions, Phys. Lett. **99B**, 333 (1981).
[58] D. Weingarten, Monte Carlo evaluation of hadron masses in lattice gauge theories with fermions, Phys. Lett. **109B**, 57 (1982).
[59] J. F. Haase, L. Dellantonio, A. Celi, D. Paulson, A. Kan, K. Jansen, and C. A. Muschik, A resource efficient approach for quantum and classical simulations of gauge theories in particle physics, Quantum **5**, 393 (2021).
[60] C. W. Bauer and D. M. Grabowska, Efficient representation for simulating $U(1)$ gauge theories on digital quantum computers at all values of the coupling, arXiv:2111.08015.
[61] T. Blum, C. E. DeTar, U. M. Heller, L. Karkkainen, K. Rummukainen, and D. Toussaint, Thermal phase transition in mixed action SU(3) lattice gauge theory and Wilson fermion thermodynamics, Nucl. Phys. **B442**, 301 (1995).
[62] U. M. Heller, SU(3) lattice gauge theory in the fundamental adjoint plane and scaling along the Wilson axis, Phys. Lett. B **362**, 123 (1995).
[63] U. M. Heller, More on SU(3) lattice gauge theory in the fundamental adjoint plane, Nucl. Phys. B, Proc. Suppl. **47**, 262 (1996).
[64] M. Hasenbusch and S. Necco, Lattice artefacts in SU(3) lattice gauge theory with a mixed fundamental and adjoint plaquette action, Nucl. Phys. B, Proc. Suppl. **140**, 743 (2005).
[65] M. Lüscher, Properties and uses of the Wilson flow in lattice QCD, J. High Energy Phys. 08 (2010) 071; 03 (2014) 092 (E).
[66] B. Berg and A. Billoire, Glueball spectroscopy in four-dimensional SU(3) lattice gauge theory (I), Nucl. Phys. **B221**, 109 (1983).
[67] B. Berg and A. Billoire, Glueball spectroscopy in four-dimensional SU(3) lattice gauge theory (II), Nucl. Phys. **B226**, 405 (1983).
[68] C. J. Morningstar and M. J. Peardon, Glueball spectrum from an anisotropic lattice study, Phys. Rev. D **60**, 034509 (1999).
[69] U. Wenger, Lattice gauge theory with fixed point actions, Ph.D. thesis, Universität Bern, 2000.
[70] Y. Chen *et al.*, Glueball spectrum and matrix elements on anisotropic lattices, Phys. Rev. D **73**, 014516 (2006).
[71] A. Athenodorou and M. Teper, The glueball spectrum of SU(3) gauge theory in $3+1$ dimensions, J. High Energy Phys. 11 (2020) 172.
[72] C. Morningstar and M. J. Peardon, Analytic smearing of SU(3) link variables in lattice QCD, Phys. Rev. D **69**, 054501 (2004).
[73] R. Brett, J. Bulava, D. Darvish, J. Fallica, A. Hanlon, B. Hörz, and C. Morningstar, Spectroscopy from the lattice: The scalar glueball, AIP Conf. Proc. **2249**, 030032 (2020).
[74] C. Culver, M. Mai, R. Brett, A. Alexandru, and M. Döring, Three pion spectrum in the $I=3$ channel from lattice QCD, Phys. Rev. D **101**, 114507 (2020).
[75] A. Francis, O. Kaczmarek, M. Laine, T. Neuhaus, and H. Ohno, Critical point and scale setting in SU(3) plasma: An update, Phys. Rev. D **91**, 096002 (2015).
[76] T. D. Cohen, H. Lamm, S. Lawrence, and Y. Yamauchi, Quantum algorithms for transport coefficients in gauge theories, Phys. Rev. D **104**, 094514 (2021).
[77] D. Banerjee, M. Dalmonte, M. Muller, E. Rico, P. Stebler, U. J. Wiese, and P. Zoller, Atomic Quantum Simulation of Dynamical Gauge Fields Coupled to Fermionic Matter: From String Breaking to Evolution after a Quench, Phys. Rev. Lett. **109**, 175302 (2012).
[78] D. Banerjee, M. Bögli, M. Dalmonte, E. Rico, P. Stebler, U. J. Wiese, and P. Zoller, Atomic Quantum Simulation of U(N) and SU(N) Non-Abelian Lattice Gauge Theories, Phys. Rev. Lett. **110**, 125303 (2013).
[79] D. Marcos, P. Widmer, E. Rico, M. Hafezi, P. Rabl, U. J. Wiese, and P. Zoller, Two-dimensional lattice gauge theories with superconducting quantum circuits, Ann. Phys. (Amsterdam) **351**, 634 (2014).

[80] E. Rico, M. Dalmonte, P. Zoller, D. Banerjee, M. Bögli, P. Stebler, and U. J. Wiese, SO(3) "nuclear physics" with ultracold gases, Ann. Phys. (Amsterdam) **393**, 466 (2018).

[81] K. Symanzik, Continuum limit and improved action in lattice theories. I. Principles and $\varphi^4$ theory, Nucl. Phys. **B226**, 187 (1983).

[82] M. Luscher and P. Weisz, On-shell improved lattice gauge theories, Commun. Math. Phys. **97**, 59 (1985); **98**, 433(E) (1985).

[83] M. Luscher and P. Weisz, Computation of the action for on-shell improved lattice gauge theories at weak coupling, Phys. Lett. **158B**, 250 (1985).